







Intermittent non-axial dipolar-field dominance of twin Laschamp excursions

Masayuki Hyodo ^{1,2✉}, Takeshi Nakagawa ³, Hayato Matsushita², Ikuko Kitaba³, Keitaro Yamada ³, Shota Tanabe², Balázs Bradák ^{1,4}, Masako Miki², Danielle McLean^{5,6}, Richard A. Staff ⁷, Victoria C. Smith ⁵, Paul G. Albert⁶, Christopher Bronk Ramsey ⁵, Akiteru Yamasaki⁸, Junko Kitagawa⁹ & Suigetsu 2014 Project*

Geomagnetic excursions represent the dynamic nature of the geodynamo. Accumulated palaeomagnetic records indicate that such excursions are dominated by dipolar-fields, but exhibit different structures. Here we report a palaeomagnetic record from the varved sediments of Lake Suigetsu, central Japan, which reveals fine structures in the Laschamp Excursion and a new post-Laschamp excursion that coincides with the $\Delta^{14}\text{C}$ maxima. The record's high-resolution chronology provides IntCal20 mid-ages and varve-counted durations. Both excursions comprise multiple subcentennial directional-swings. Simulations of filtering effects on sediment-magnetisations demonstrate that this high-resolution record replicates most of the features in existing, lower-resolution Laschamp excursion records, including the apparent clockwise open-loop of the virtual geomagnetic pole pass. The virtual geomagnetic poles during the 'swing' phases make four clusters centred in hemispherically-symmetric regions, three of which encompass the virtual geomagnetic poles associated with the Laschamp Excursion recorded in lavas at various locations. The stationary dipolar-field sources under each cluster should have intermittently dominated one after another during the excursions.

¹Research Center for Inland Seas, Kobe University, Kobe 657-8501, Japan. ²Department of Planetology, Kobe University, Kobe 657-8501, Japan. ³Research Centre for Palaeoclimatology, Ritsumeikan University, Kusatsu, Shiga 525-8577, Japan. ⁴Graduate School of Maritime Sciences, Kobe University, 5-1-1 Fukaeminami-machi, Higashinada-ku, Kobe 658-0022, Japan. ⁵School of Archaeology, University of Oxford, 1 South Parks Road, Oxford OX1 3TG, UK. ⁶Department of Geography, Swansea University, Abertawe, UK. ⁷Scottish Universities Environmental Research Centre (SUERC), University of Glasgow, East Kilbride G75 0QF, UK. ⁸Fukui Prefectural Satoyama-Satoumi Research Institute, Wakasa-cho, Mikatakaminaka-gun, Fukui 919-1331, Japan. ⁹Varve Museum, Wakasa-cho, Mikatakaminaka-gun, Fukui 919-1331, Japan. *A list of authors and their affiliations appears at the end of the paper. ✉email: mhyodo@kobe-u.ac.jp

The geomagnetic field occasionally deviates in a direction far beyond the range of secular variation. Such events are termed geomagnetic excursions, usually defined as a temporary deviation of a field direction whose virtual geomagnetic pole (VGP) deviates more than 45° from the geographical pole¹. Geomagnetic excursions, together with reversals, represent the dynamic nature of the geodynamo at times when the dipole field strength decreases to less than half of the present value². Geomagnetic excursions typically occur at intervals of 10^4 to 10^5 yr³, but their internal structure has rarely been observed in sediment-magnetisations, time-averaged geomagnetic field records, due to their short duration (typically less than ca. 2 kyr). Therefore, palaeomagnetic data of excursions are still insufficient and geographically biased, making it difficult to analyse such an event on a global scale. Moreover, very few datasets⁴ resolve subcentennial structure of excursions, with some excursions terminating within just a few hundred years.

The Laschamp Excursion was first discovered in the magnetisations of lava flows from the Chaîne des Puys, France⁵, and further investigations confirm a deviation in the magnetic field^{6,7}. This excursion was subsequently recognised in other lavas in Iceland^{8,9} and New Zealand^{10,11}, as well as in deep-sea sediments^{12–15}, Chinese loess sequences¹⁶, a speleothem¹⁷, and lake sediments¹⁸. The lavas that record the excursion have been $^{40}\text{Ar}/^{39}\text{Ar}$ dated to between 40 and 46 kyr BP^{11,19}. The dates are consistent with the estimated mid-point ages of between 40 and 43 kyr BP identified in sediments based on $\delta^{18}\text{O}$ stratigraphy, climatostratigraphy, and/or ^{14}C -, optically-stimulated luminescence- and U–Th-dating^{4,13,16,17}. The estimated duration for an excursions-direction interval, on the other hand, vary across a wide range, grouping at 200–300, 400–500 and >900 yr (Supplementary Table 1). In spite of this difference, the sedimentary records exhibit many common features, such as the precursor immediately (<500 yr) predating the main excursion^{4,14} and the clockwise open loop of the VGP-pass^{4,15}. Therefore, the variability of the estimated duration possibly arises from inaccuracy of chronology and the filtering effects of low-resolution data series, other than regional variabilities^{20,21}. Precisely dated, high-resolution records of the Laschamp Excursion, therefore, have been highly anticipated to reconcile these ambiguities. Well-dated Laschamp Excursion records that comprise multiple excursions directions (Supplementary Table 1) have seldom been reported from sedimentary archives with a sedimentation rate (s.r.) lower than ca. 20 cm/kyr, which is thought to be smoothing the post-depositional remanent magnetisation (PDRM) signal^{22,23}. High-resolution records are also anticipated from cosmic ray studies associated with excursions^{24,25}.

The varved sediment of Lake Suigetsu (Supplementary Fig. 1) has the potential to provide a well-dated, high-resolution temporal dataset through the Laschamp Excursion. It is one of the most precisely age-controlled sedimentary archives in the world^{26,27}, with annual layers (varves) counted by dual methods^{28–30} as well as >800 radiocarbon dates obtained on terrestrial leaf fossils^{27,31}. The dataset has been used as a central component of the IntCal13 and IntCal20 radiocarbon calibration models^{32,33}. The age uncertainties (1σ) given to the Suigetsu sediment at around the expected Laschamp Excursion are only ± 60 – 100 -yr, and the mean s.r. of 90–100 cm/kyr during this period is very high compared with many other sedimentary records (Supplementary Table 1). The preservation of varves provides support that a good palaeomagnetic record can be expected from the sediments, which should have acquired magnetisations unaffected by bioturbation. In this article, we report the high (21-yr) resolution palaeomagnetic record from Lake Suigetsu varved sediments that reveal decadal structures of the Laschamp Excursion with a duration of 790 varve years and a

new excursion with a duration of 550 varve years about 2600-yr postdating the Laschamp Excursion. These excursions comprise multiple subcentennial directional-swings caused by four stationary non-axial dipolar sources intermittently dominated one after another in clockwise order.

Results and discussion

The Laschamp and new post-Laschamp excursions. High-resolution samples (every 2-cm depth around excursions) for magnetic analyses were taken from the varved “SG14” Lake Suigetsu sediment core (Methods). We use a characteristic remanent magnetisation (ChRM) isolated between 200 and 450–590 °C from each sample (Supplementary Discussion, and Supplementary Figs. 2 and 3). It is regarded as a primary natural remanent magnetisation (NRM) carried mainly by detrital magnetites (Supplementary Discussion and Supplementary Fig. 2). The ChRMs reveal two intervals of excursion comprising multiple swings of directions whose VGPs deviate $>45^\circ$ from the North Pole (Fig. 1, Supplementary Figs. 4, 5, and Supplementary Data 1). Based on the Bayesian age model^{31,34}, the lower excursion ranges from 42,400–41,700 IntCal20 yr BP and the upper one from 39,090–38,580 IntCal20 yr BP (Figs. 1 and 2). The lower excursion consists of five swings, and the upper one consists of two. We label these swings A, B, C, D, E, F and G in ascending order (Fig. 1). The non-excursion field represented by a single sample between swings D and C exhibits full normal polarity with a VGP latitude of 80.7°N , hence we separate D and C with confidence. On the other hand, the non-excursion fields within swings A and G have near excursion VGPs with latitudes 47.4 and 57.2°N , respectively, and thus we regard them as a single episode. However, the possibility remains that there were shorter episodes of full normal polarity that were not detected due to the analytical resolution. The duration of each swing, including the thickness of a discrete sample (2 cm), ranges from 18 to 160-yr (based on varve counts; Table 1).

The lower excursion comprising swings A–E is correlated with the 40–46 kyr Laschamp Excursion including the precursor^{4,11,19}. The mid-age of $42,050 \pm 120$ IntCal20 yr BP from the Lake Suigetsu record and a varve-counted duration of 790 yr are the best estimates yet for the Laschamp Excursion, from the high-resolution and precisely age-controlled palaeomagnetic data (Supplementary Table 1). In addition, the upper excursion, with a mid-age of $38,830 \pm 140$ IntCal20 yr BP and a varve-counted duration of 550 yr (Table 1), has not been previously recognised. The Mono Lake Excursion, dated to between 32 and 35 kyr BP^{13,18}, is too young to be a counterpart of it, and no other excursions based on high-precision data have been reported from elsewhere between 35 and 40 kyr BP. However, some lava-flow excursion records in France⁷ may correlate with the upper excursion (swings F and G) as well as swing E.

The relative palaeointensity (Methods, Supplementary Data 2) provides minima around both excursions and a gentle rise between them with a peak closer to the younger excursion (Fig. 1d). The palaeointensity variation resembles that of the Black Sea record between ca. 41.5 and 39 ka on its climatostratigraphic age scale⁴ (Fig. 1h), although no excursion-direction is recorded or resolved at the younger minimum. The younger excursion appears to be a rebound of the Laschamp, displaying similar characteristics. The large decrease of palaeointensity during excursions causes an increase in the cosmic ray flux, therefore, an increase in the production rates of cosmogenic nuclides in the stratosphere^{24,25}. The production rates of nuclides ^{10}Be and ^{14}C would have elevated during the Laschamp Excursion. However, the $\Delta^{14}\text{C}$ measured in various archives is delayed relative to the ^{14}C production as it is filtered and

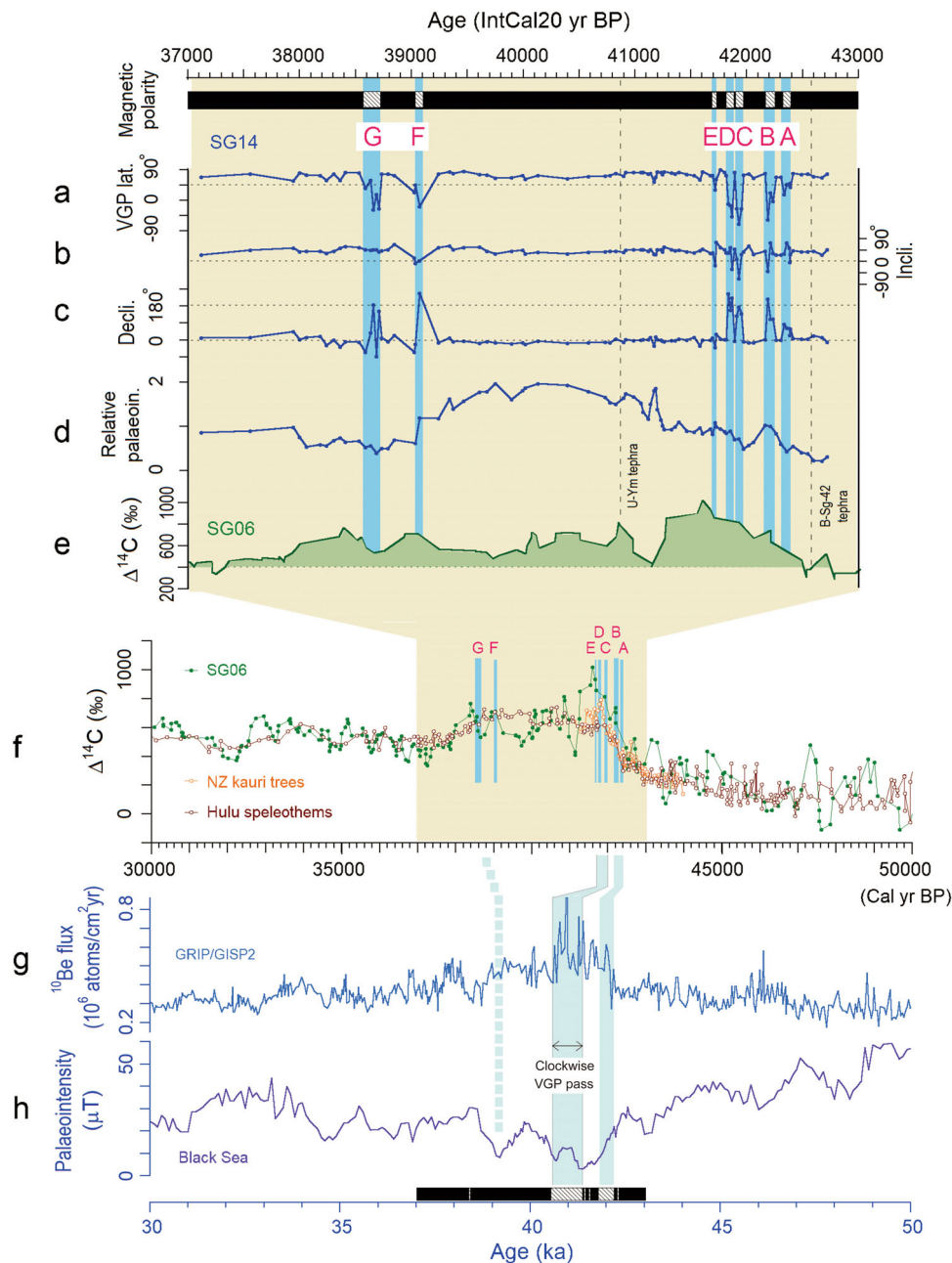


Fig. 1 High-resolution palaeomagnetic data from Lake Suigetsu (a–d) and comparison with other data. Time variations of VGP latitudes (a) and inclinations (b) and declinations (c) of ChRMs, and the relative palaeointensity ($J_{200^\circ\text{C}}/\chi_{200^\circ\text{C}}$) normalised to a total mean (d). The successive swings are labelled ‘A–G’ (see text). e Weighted five-point moving averaged $\Delta^{14}\text{C}$ data from Lake Suigetsu^{31,34}. The dashed lines represent depositional ages of the key chronostratigraphically relevant volcanic ash (tephra) fall events identified in the SG14 core⁵⁷. f $\Delta^{14}\text{C}$ data spanning 30,000 to 50,000 cal yr BP from Lake Suigetsu^{31,34}, New Zealand kauri trees²⁵ and Hulu cave speleothems³⁶. The graphs of (a–e) and the Lake Suigetsu $\Delta^{14}\text{C}$ of (f) are plotted against IntCal20 yr BP. The age values in cal yr BP in (f) are based on ^{14}C -dating and tree-ring counting for kauri trees and U–Th dating for speleothems. g ^{10}Be flux data from Greenland ice cores plotted against the GICC05 age model⁶⁰. h Palaeointensity data from Black Sea sediments plotted against an age model climatologically correlated to the GICC05 age model⁴. In the magnetic polarity based on the VGP latitude, the black/hatched zones show normal-polarity/excursion intervals.

attenuated in amplitude as it makes its way through the global carbon cycle between atmosphere, biosphere, and the ocean, whereas ^{10}Be directly reflects cosmic ray intensity variations with almost no attenuation and a delay of only 1–2 yr³⁵. Concomitant $\Delta^{14}\text{C}$ in Lake Suigetsu is very high (>400‰) during the intervals of the Laschamp and the post-Laschamp excursions, supported by other $\Delta^{14}\text{C}$ data from other sites^{24,25} (Fig. 1e, f). In addition, the extremely high (>600‰) $\Delta^{14}\text{C}$ peaks just postdate swings A–E, F and G, by 300–400 yr, ca. 50 yr and ca. 250 yr, respectively.

These time lags, likely dependent upon frequencies of variations, are comparable with simulation estimates from a 12-box model³⁷. Thus, the cosmic ray flux probably increased in phase with the excursions even on decadal-centennial time scales. The high cosmic ray flux during the Laschamp Excursion is also evidenced by the high ^{10}Be flux in Greenland ice cores compared with the Black Sea palaeomagnetic data⁴ (Fig. 1g, h). As discussed below, the main excursion and the precursor in the Black Sea record can be correlated with a combined swing of C and D, and B (or

A + B) in Lake Suigetsu, respectively. These correlations would be useful for connecting the ice core age model (GICC05) and the IntCal20 age model, which is beyond the scope of this study.

The post-Laschamp excursion record from Lake Suigetsu sediments provides a chronologically important geomagnetic-directional episode that postdates the widespread 'U-Ym' tephra by ca. 1700 years (see Methods for further details), and is separated from the main Laschamp excursion by ca. 2600 years. Here, we propose to name this the 'Post-Laschamp (Suigetsu) Excursion' for the convenience of chronological application.

Corroboration from existing lower resolution records. The detailed structure of the Laschamp Excursion that we recognise in the Suigetsu core, comprising multiple subcentennial episodes, is

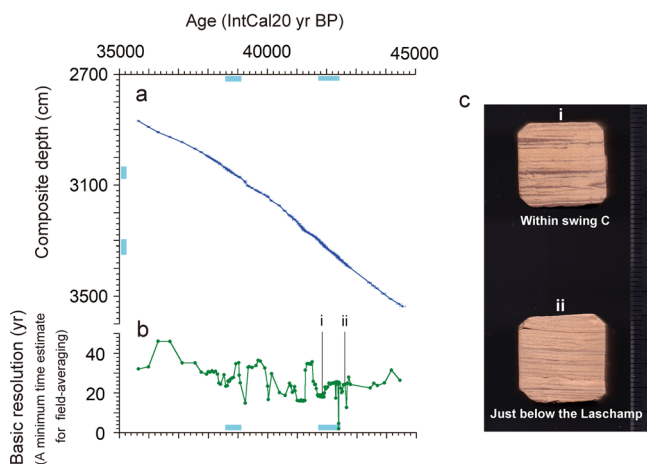


Fig. 2 Age model for core SG14. **a** The age versus composite-depth plot for mid-depths of all palaeomagnetic samples, based on the correlation model: version 06 Apr. 2020. The error bars show $\pm 1\sigma$ errors. The blue bars represent the intervals of the Laschamp (lower) and the post-Laschamp (upper) excursions. **b** The time variation of a basic resolution for each sample (a minimum time estimate for field-averaging) is calculated by dividing the thickness of a sample (2 cm) by a s.r. between adjacent sample levels. The low basic-resolution values are from core segments from parallel boreholes (3189 cm) and event (flood) layers (3350, 3358–3360 and 3384 cm). **c** Cross-section photographs of dry cubic samples after progressive THDs within Swing C of the Laschamp (i) and just below the Laschamp Excursion (ii). The original wet thickness of the sample is 2 cm (dry thickness is ca. 1.8 cm).

unique. The simpler behaviour shown by previous, lower s.r. (20–44 cm/kyr) records (Supplementary Table 1), may be the consequence of the filtering effects of a greater PDRM process associated with lower sedimentation rates, as well as the direct loss of sampling resolution. First, we simulated how the present magnetisation data would be smoothed in records with lower s.r., without filtering by a PDRM process. The time-series vectorial data (Methods) were condensed for sediments with various s.r. assuming that magnetisations were measured on 2-cm thick (Δt -yr spanning) samples taken at 2-cm (Δt -yr) intervals. Here, we define Δt ($=2$ cm/s.r.) as a basic resolution (a minimum time estimate for field-averaging). Δt is 21-yr for the Lake Suigetsu sediments, consistent with the visual varve counts with dried samples after thermal demagnetisations (THDs) (Fig. 2). The condensation is equivalent with convolution integration (or filtering) with a box function with a width of Δt , with every- Δt outputs. For simulations, we used the time-series data of the orthogonal three magnetisation components converted from declination, inclination and relative palaeointensity (Fig. 3, Methods). Figure 3a shows curves of VGP latitude and relative palaeointensity calculated from the outputs for a s.r. of 48, 40, 20, 12 and 9 cm/kyr. When the s.r. is halved (48 cm/kyr), swing E disappears, and swings C and D are combined (tentatively named 'CD'). The large swing CD still remains at 12 cm/kyr, but disappears at 9 cm/kyr. The presence of excursions signals even at 12 cm/kyr is inconsistent with real data from sediments with s.r. < 20 cm/kyr as almost none exhibit any Laschamp-related excursion-direction signals. Such sediments are most likely to have undergone filtering of magnetisations by a PDRM process.

A PDRM is a time-averaged geomagnetic field filtered with a magnetisation lock-in rate function^{38–40}. Therefore, dually filtered sediment-magnetisations can be calculated using the lock-in rate function and a box function. We simulated the filtering effect for a fixed s.r. with various values of $Z_{1/2}$ ($T_{1/2}$), a half lock-in depth (time) where 50% of a magnetisation is locked-in³⁸ (Methods, Supplementary Fig. 6). In the VGP latitude curves for a s.r. of 44 cm/kyr (the highest value for the previous sedimentary records spanning the Laschamp Excursion), at 0.5 cm for $Z_{1/2}$, swing E disappears, and a combined swing 'CD' appears (Fig. 3b). Swing A just disappears at 1 cm, B at 2 cm and CD at 4 cm. The excursion comprising swings B and CD at $Z_{1/2}$ of 1.0 and 1.5 cm spans about 450 yr, which correlates well with the double-episode Laschamp Excursion spanning 400–500 yr recorded in the North Atlantic^{12,14}. The excursion with only CD at $Z_{1/2}$ of 2.0 cm spans about 140-yr, which can be correlated with the single-episode Laschamp Excursion spanning 200–300 yr

Table 1 Depth ranges, mid-ages and durations of excursions and swings from Lake Suigetsu varved sediments.

Excursion/swing	Composite depth range (cm)	Mid-age	Duration (yr)		SG06 ₂₀₁₈ vyr
		IntCal20 yr BP	IntCal20 (Lower, Upper)		
Laschamp Excursion	3,363.0–3,296.0	42,050 ± 120	696 (–100, +106)		794
Swing A	3,363.0–3,352.7	42,360 ± 120	83 (–13, +3)		88
Swing B	3,346.6–3,340.6	42,210 ± 120	75 (–19, +1)		71
Swing C	3,322.7–3,316.7	41,930 ± 130	64 (–8, +12)		64
Swing D	3,314.7–3,308.7	41,850 ± 120	56 (–0, +20)		58
Swing E	3,298.0–3,296.0	41,720 ± 120	20 (–1, +5)		18
*Post-Laschamp (Suigetsu) Excursion	3,073.0–3,036.6	38,830 ± 140	509 (–68, +54)		546
Swing F	3,073.3–3,068.1	39,050 ± 130	79 (–16, +1)		91
Swing G	3,048.4–3,036.6	38,650 ± 140	145 (–2, +38)		160

*Named in this study. Depth and age ranges for each swing include the thickness of excursion samples at either end. Uncertainties in the IntCal20 age model^{31,34} are presented at 2σ . The values of mid-ages and errors are rounded. Varve count durations (SG06₂₀₁₈ vyr) are estimated from the varve chronology³⁰.

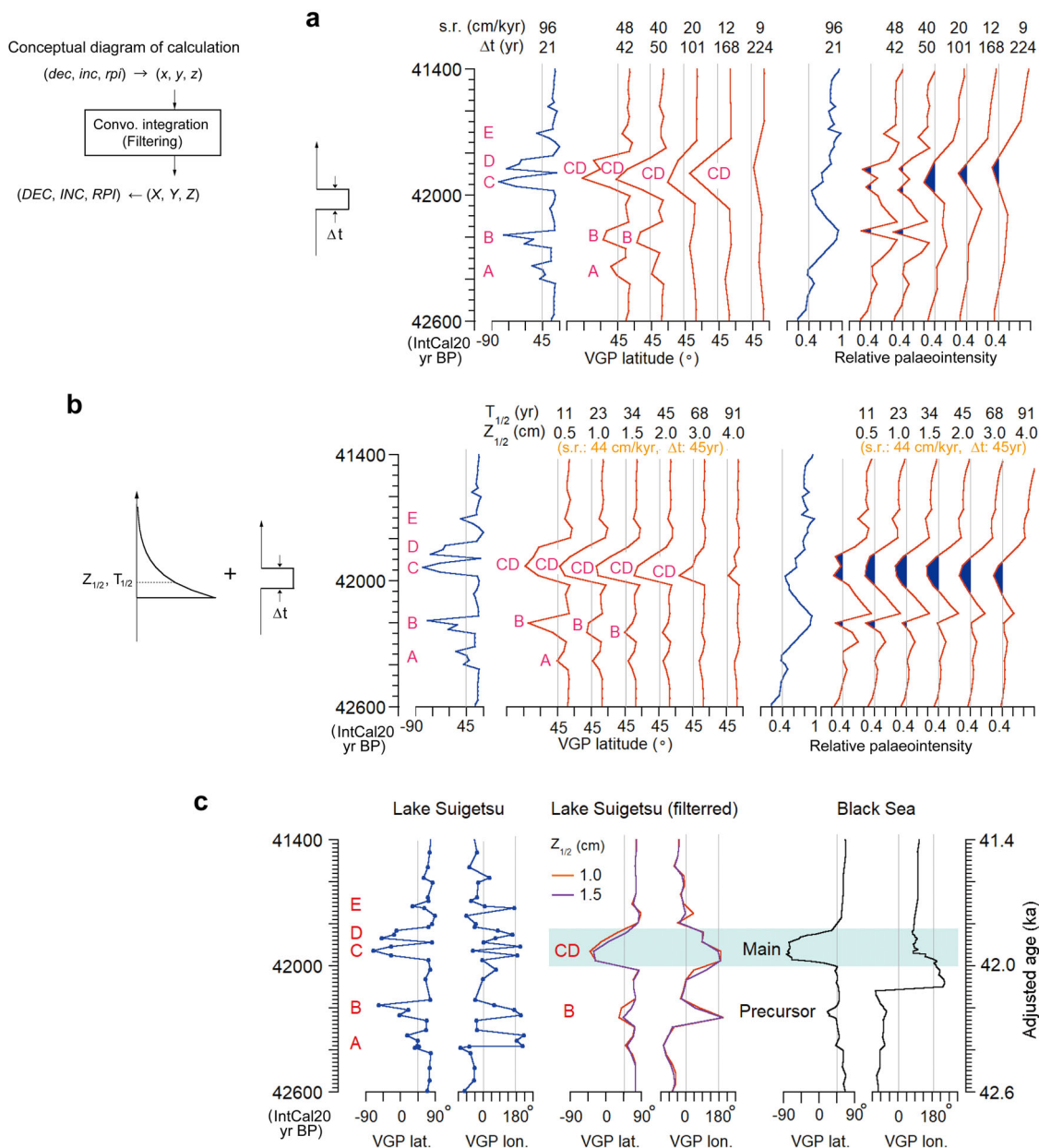


Fig. 3 Simulated results to illustrate the filtering effect if our high (21-yr) resolution Lake Suigetsu magnetisation data had instead been recorded in lower s.r. sediments. a VGP latitude and palaeointensity curves from the Lake Suigetsu magnetisation vector (x, y, z) data condensed to every Δt (2 cm/s.r.)-yr data (equivalent with filtering with a box function with a width of Δt) for various s.r. **b** VGP latitude and palaeointensity curves from the Lake Suigetsu magnetisation vector (x, y, z) data convolution-integrated with an exponential lock-in rate function defined by a half lock-in depth/time ($Z_{1/2}/T_{1/2}$), and condensed to every Δt -yr data (equivalent to the dual filtering with an exponential lock-in rate function and a box function). The calculations are made with various $Z_{1/2}/T_{1/2}$ values for s.r. of 44 cm/kyr, the highest value for the previous sedimentary records of the Laschamp Excursion (Supplementary Table 1). The dark blue areas represent obvious artefacts of palaeointensity decreases <0.4 , produced by the convolution integration. **c** VGP latitude and longitude curves of the Lake Suigetsu data before and after filtering, and the Black Sea data⁴. The light cyan bar represents the interval of the clockwise open-loop VGP-pass. ‘A–E’ and ‘CD’ on the VGP latitude curves represent excursions swing episodes.

in China and the North Atlantic^{16,41}. The swing CD at $Z_{1/2}$ of 3 cm spanning <50 yr would be difficult to detect. A $Z_{1/2}$ of 1.0–1.5 cm for natural sediments is realistic, whereas that of >2 cm is not (Methods)^{23,42,43}. The output VGP latitude and longitude variations for CD correlate well with those for the main excursion seen in the Black Sea record⁴ (Fig. 3c), which indicates the dominance of non-axial dipolar fields. For the remaining interval, they disagree with each other, except the output swing B that can be correlated with the precursor in the Black Sea; the VGP variation has a comparable signal in latitude but does not in

longitude, which may be caused by a filtering effect due to the low s.r. (20–30 cm/kyr) or reflect regional fields.

The relative palaeointensity curves in any simulations have remarkable drops, by 70–80% at their maximum, around swings B, C and D (Fig. 3a, b). These swings include largely deviated fields with VGPs in the southern high-latitudes. The vector sum of such nearly-reversed and normal-polarity magnetisation components forges an apparent large decrease of palaeointensity. We should note that sediment-magnetisation intensity more or less contains such forged decrease components, which sometimes

largely lowers the palaeointensity value and may even shift a minimum in position (time), especially around geomagnetic excursions and reversals³⁸ (Supplementary Fig. 6). Relative palaeointensity artefacts are introduced even by NRM acquisition efficiency variations in terms of remanence carrier alignment and magnetic components with different intrinsic ratios between their NRM contributions and a magnetisation normaliser^{40,44}. In the Black Sea data (Fig. 1h), the palaeointensity takes a flat value of ca. 12 μ T, about 1/4 of the present field intensity, around the centre of the main excursion that coincided with the cosmic ray peak. However, the wide interval of palaeointensity values much lower than 12 μ T with a minimum of 3 μ T, predates the flat interval, centred between the main excursion and the precursor (Fig. 1h). This extremely low palaeointensity interval, without a corresponding much higher cosmic ray increase (Fig. 1g), may be an artefact. Careful interpretations of sediments' palaeointensity records are always necessary, including even the present Lake Suigetsu data. The minor peaks of $\Delta^{14}\text{C}$ between ca. 41,000 and 40,000 IntCal20 yr BP (Fig. 1d, e) are not reflected in the palaeointensity curve, which indicates the collapse of inverse correlations between palaeointensity and $\Delta^{14}\text{C}$ changes. We need more datasets to assess the correlation during this extremely low palaeointensity period.

VGPs longitudinally constrained pass and clockwise shifting cluster. The VGP-path is constrained to longitudinal bands through the Pacific Ocean for swings A and C, and eastern Africa-the Indian Ocean for swings D, E and F (Fig. 4a). The VGPs of swings B and G arrived in eastern Africa-Indian Ocean band via the Pacific band, returning to northern high-latitudes through different bands. Swing C reached the highest southern latitude (71.3°S) within 43 kyr. Such a rapid near-reversal can only occur in the field in the Earth's liquid outer core, which reverses in direction on time scales of 500-yr or less⁴⁵. During the Laschamp Excursion, rapid near-reversals occurred within 20–45 kyr in swings B, C and D. It is noteworthy that the excursions VGPs of lava flows from France, Iceland, New Zealand, and Japan related to the Laschamp Excursion are in or near those bands recognised in Lake Suigetsu (Fig. 4a).

The excursions VGPs make clusters centred in the North Pacific (NP), the South Pacific (SP), the Southern Indian Ocean (SI) and eastern Africa (EA) (Fig. 4b). In addition, most VGPs of lava flows from various locations fall into one of these clusters, except for the SI cluster. The clustering of VGPs from distant (>9000 km) sites indicates that the excursions are dominated by dipolar fields possibly originating from near-radial negative flux concentrations under each cluster. The dipolar source under the NP cluster, whose magnetic north pole locates under the NP, dominated swings A and B, followed by the dominance of the source under the SP during swing C. The source under the SI mainly dominated swing D, and partly swings B and F. The source under the EA dominated swing E. This source recovered ca. 2,600-yr later, to dominate swings F and G. Those sources became dominant generally in clockwise order from the NP to EA, with sporadic extra dominances by the source under the SI. In addition, each dominance interval is relatively short (<ca. 100 kyr). The non-excursion intervals dominated by geocentric axial-dipole fields between swings are rather long (240 kyr maximum). The VGPs of swings B, D and F dropped in the SI cluster and left it very swiftly. Thus, dipolar-source dominances in the SI cluster were intermittent and short in duration, which might make instantaneous spot-recordings of excursions unlikely for lava flows. The dipolar sources may correlate with the negative flux concentrations at the core-mantle boundary (CMB) in the spherical harmonic (SH) field models of the Laschamp

Excursion^{46,47}, whose positions agree well with the four VGP clusters. The models are mainly based on low-resolution deep-sea palaeomagnetic data. Therefore, the flux concentrations at the CMB reflect the features of relatively long-time-averaged fields during the excursion. Due to the low temporal resolution, the SH models do not resolve the frequent normal polarity (non-excursion) field dominances between swings that are observed in the Lake Suigetsu data. In addition, the SH models have an extra concentration under the low-latitude North Atlantic, which may reflect the uneven geographical distribution of the contributing palaeomagnetic data.

The filtered data represent a large open clockwise loop of VGP, consistent with the data from Black Sea sediments^{4,48}, although the southernmost VGPs somewhat shift northward by filtering (Fig. 4c). The two datasets should have captured the same high-cut filtered field-behaviours of the main Laschamp Excursion. However, the absolute age ranges are somewhat discordant, probably ascribed to the application of different dating methods; i.e., the chronology of the Black Sea data is based on climatic wiggle matching. The multi-core data stack from the Black Sea has an analytical interval of ca. 10-yr, but the basic resolution is 50–80-yr (Supplementary Table 1), with which it is difficult to resolve subcentennial swings. Many sedimentary records of the Laschamp Excursion show similar open clockwise VGP-loops from high northern latitudes through the Pacific Ocean to high southern latitudes, with a return through the Indian Ocean and Africa back to high northern latitudes. The records of the Iceland Basin Excursion at about 190 kyr³ show an open anticlockwise VGP-loop through the same pass^{15,49}. The consistent open clockwise VGP-passes show evidence for the dipolar-field dominance during the Laschamp Excursion. In addition, the consistent VGP-passes shown by different excursions (Laschamp and Iceland Basin) indicate the stationary dipolar-sources recurrently dominated in the same manner.

The four dipolar-field sources (under the NP, the SP, the SI and the EA), correlated with the negative flux concentrations at the CMB of the SH model^{46,47}, are similar to the four stationary high-latitude radial-flux concentrations at the CMB (over Canada, the South Pacific, the Southern Indian Ocean, and Eurasia) that have repeatedly waxed and waned on decadal-centennial time scales throughout the past 3-kyr⁵⁰ (Fig. 4d). The hemispherically-symmetric pattern of four stationary flux concentrations may have persisted even during the excursions, provided that the latitudes somewhat lowered and the southern-latitude concentrations reversed in sign. The latter behaviour (sign reversal) is probably common with geomagnetic reversals, and has not occurred in the past 3-kyr of secular variation. The persistence of stationary radial-flux concentrations can be caused by the influence of mantle heterogeneity in thermal core-mantle coupling^{51,52}. The SH models represent no clockwise-order waxing and waning of the stationary radial-flux concentrations at the CMB, due to the low-resolution of data used^{46,47}. However, the flux concentration under the NP predominated in the early stage of the excursion, and that under the EA slightly dominated in the final stage, which possibly concerned swings A/B and E, respectively. Thus the SH models may partly support the clockwise order dominance of dipolar sources.

The VGPs exhibited by three discrete samples dropped in a minor cluster around eastern Australia (Fig. 4b) may represent a transit cluster or a part of an expanded SP or SI. The cluster is near the region where a minor, negative radial-flux concentration has sometimes appeared at the CMB during the late Holocene⁵⁰. This region overlaps with a cluster of transitional VGPs of lava flows and sediments with high s.r. associated with the Matuyama–Brunhes polarity reversal^{53,54}. This may be evidence of a persistent stationary radial-flux concentration around the

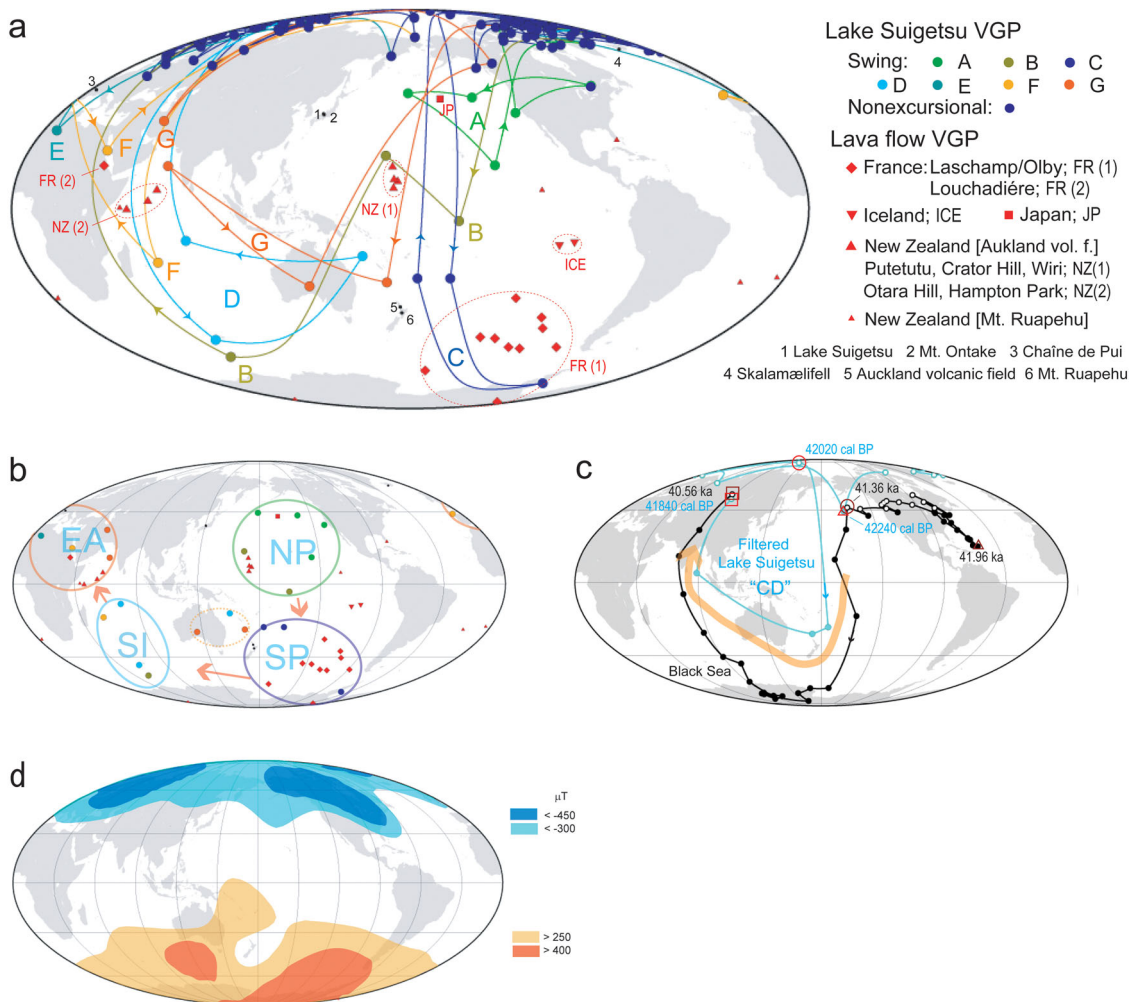


Fig. 4 Mollweide projection of VGPs centred on 180° longitude. **a** VGP-path for the Laschamp to the post-Laschamp excursions, as recorded in Lake Suigetsu, and excursive VGPs from lava flows related to the Laschamp Excursion. The lava-flow VGPs are from France^{6, 7, 19}, Iceland^{9, 61}, New Zealand^{10, 11, 62} and Japan⁶³. The small black numbered dots show the sites of samples. **b** VGP clusters for the Laschamp Excursion centred in the North Pacific (NP), the South Pacific (SP), the Southern Indian Ocean (SI) and eastern Africa (EA). The dotted circle indicates a possible cluster (see text) around Australia. The symbols are the same as (a). **c** Comparison of VGP paths. Aqua colour; the Lake Suigetsu data filtered with an exponential lock-in rate function with a $Z_{1/2}$ of 1.5 cm and condensed to a resolution of 45-yr per data point (Fig. 3b). Black colour; the Black Sea Laschamp data^{4, 48}. The solid/open circles represent excursive/non-excursive VGPs. The red/brown open symbols represent the peak of the precursor (triangle), the start (circle) and the end (square) of the main excursion for the Lake Suigetsu/Black Sea data. **d** Time-averaged radial field component at the core-mantle boundary of the time-varying spherical harmonic model (CAL3k.4b) spanning 1000 BC to AD 1990 (adapted from ref. 50).

region, coupled with the core-mantle dynamics^{55,56}. Thus, this minor cluster is a feature common with the Matuyama–Brunhes reversal, as well as the geomagnetic secular variation.

Summary. The palaeomagnetic record from the varved sediments of Lake Suigetsu (SG14) reveals a sub-structure associated with the Laschamp Excursion at a high chronological resolution, as well as a new post-Laschamp excursion, tentatively named here the ‘Post-Laschamp (Suigetsu) Excursion’. The mid-ages and the varve-counted durations are $42,050 \pm 120$ IntCal20 yr BP and 790 SG06₂₀₁₈ vvr for the Laschamp Excursion, and $38,830 \pm 140$ IntCal20 yr BP and 550 SG06₂₀₁₈ vvr for the Post-Laschamp (Suigetsu) Excursion, respectively, coincident with the cosmic ray flux proxy ($\Delta^{14}C$) maxima, with time lags induced by the global carbon cycle. Our data reveal that both excursions are characterised by multiple subcentennial field-directional swings containing rapid near-reversals within 20–45 yr. Simulations of filtering effects on sediment-magnetisations show that our high-resolution record replicates most of the features seen in previous

Laschamp Excursion records with lower s.r. The VGPs of the high-resolution Laschamp Excursion dataset make four clusters centred in the North Pacific, the South Pacific, the southern Indian Ocean, and eastern Africa, three of which include the VGP clusters seen in the snapshot records of lavas from various regions. This agreement of the VGP clusters, together with the consistent clockwise open loops of the VGP-pass among the previous low s.r. records and the filtered data of the high-resolution record of this study, demonstrate that the Laschamp Excursion was dominated by non-axial dipolar fields. The dominance of non-axial dipolar fields was intermittent, generated in clockwise order by the four stationary sources, and possibly linked to lower mantle heterogeneity.

Methods

Collection of the SG14 core from Lake Suigetsu. Lake Suigetsu is a tectonic lake with an area of about 4.3 km² and a maximum depth of 34 m, located close to the Sea of Japan coast, central Japan (Supplementary Fig. 1). The lake has no direct river influx and thus is supplied with no coarse detrital materials. Lake Suigetsu is connected to the neighbouring Lake Mikata by a shallow and narrow sill (ca. 4 m

deep, ca. 45 m wide), through which freshwater from the Hasu River, the only freshwater source to the multiple lake system, is supplied together with fine-grained detrital materials which pass through the natural filter of Lake Mikata (Supplementary Fig. 1). Lake Suigetsu has a calm water surface with virtually no high-energy flows, partly due to the protection from winds by surrounding hills, and thus forms a stable stratified water column. The absence of major vertical mixing of water results in less oxygen supply to the lake bottom, creating anaerobic environments and greatly reduced biological activity at the lake bottom. Seasonally different types of material are deposited, comprising a layer of *Aulacoseira* spp. diatoms with a small amount of siderite overlain by an aeolian dust layer in spring, a light amorphous organic material layer in summer, an *Encyonema* diatom layer overlain by a siderite layer in autumn, and a clay layer in autumn to winter²⁶. Identification of these seasonal layers, comprising varves, was the key for counting and producing an independent chronology. More than 50,000 annual layers were identified in the top 45 m of the sequence of SG06 (an earlier core retrieved from Lake Suigetsu), and sporadic event layers relating to floods, earthquakes and tephra, along with regular varve accumulation, facilitated the correlation of sections obtained from parallel boreholes²⁶.

In summer 2014, for the purpose of exhibiting varved sediments at the 'Fukui Prefectural Varve Museum' (<http://varve-museum.pref.fukui.lg.jp/en/>), the local government funded the collection of the 'SG14' sediment core (officially named 'Fukui-SG14') from the central flat plain of Lake Suigetsu, about 350 m east of the SG06 coring point (Supplementary Fig. 1). Like SG06, sections comprising SG14 core were recovered from four parallel boreholes with overlaps, ensuring that there were no gaps in the retrieved composite stratigraphy. Most of the sections are ca. 1-m long. The coring method was similar to that for the SG06 core. The total length of the composite profile of SG14 is 98.2 m, reaching the basement gravel layer. A series of core splitting and high-resolution photography of the exposed sediment cross-sections was performed in the temporary lakeshore laboratory, in parallel with the coring work on the lake. Owing to such parallel works, we could chronologically monitor each section by stratigraphic correlation with the SG06 data including high-resolution cross-section photographs, which enabled prediction of the depths of the target sections for oriented coring. The half-cut core sections were sealed immediately after they were photographed, and kept in plastic bags containing oxygen absorbent material until magnetic sampling.

Magnetic analyses. We preliminarily collected cubic sediment samples of 10 cm³ by pushing plastic boxes into the exposed core sections, followed up with retrieval of 2 cm³ × 2 cm³ × 100 cm³ LL-channel samples from each 1 m-section for the main analysis²⁶. From the LL-channel samples, 2 cm³ × 2 cm³ × 2 cm³ samples were cut using a knife at contiguous 2 cm depth intervals for excursions and 4–30 cm depth intervals for the remaining sections. We primarily took samples from the oriented core sections, but also took supplemental samples from unoriented sections. A total of 131 samples, 119 for palaeomagnetic and 12 for rock magnetic analyses, were collected from an age interval of 35 to 45 kyr (most intensively sampled from 37.9 to 42.7 kyr).

All the samples were subjected to progressive THDs at intervals of 30–50 °C up to 590–680 °C. An NRM of a sample was measured using a 2 G cryogenic magnetometer. At each step of THD, low-field magnetic susceptibility (χ) was measured using a magnetic susceptibility metre (MS2, Bartington Measurements, UK) to monitor magnetic mineral alterations. To estimate magnetic carriers, we performed thermomagnetic analyses in an air atmosphere for selected samples using an NMB-89 magnetic balance (Natsuhara Giken Corporation, Osaka, Japan). A sample was heated from 50 °C to 700 °C and then cooled to 50 °C at a rate of 10 °C/min. Isothermal remanent magnetisation (IRM) acquisition experiments and hysteresis measurements were performed for both non-heated and heated (350 °C) samples using an AGM microMag 2900 (Princeton Measurements Corporation, Westerville, OH, USA). The IRM was measured at 100 levels from 0.1 to 1000 mT. Magnetic carriers and primary NRM components based on these experiments' results are discussed in the Supplementary Discussion.

ChRMs were calculated by principal component analysis. Declinations of ChRMs were corrected by rotating the core segment frame to adjust the mean declination of viscous remanent magnetisations to the present geomagnetic north (Supplementary Discussion, Supplementary Figs. 4, 5 and Supplementary Data 1). For relative palaeointensity, the NRM intensities of samples after 200 °C- and 350 °C-THDs ($J_{200\text{ °C}}$ and $J_{350\text{ °C}}$) were normalised by the magnetic susceptibility values of samples after 200 °C- and 350 °C-THDs ($\chi_{200\text{ °C}}$ and $\chi_{350\text{ °C}}$), respectively. The ratios of $J_{200\text{ °C}}/\chi_{200\text{ °C}}$ and $J_{350\text{ °C}}/\chi_{350\text{ °C}}$ further normalised by total means were used for discussion (Supplementary Discussion, Supplementary Fig. 5 and Supplementary Data 2).

Chronology. Construction of the age-depth model for SG06 involved a three-stage process. Firstly, a pure varve (SG06₂₀₁₈ vvr) chronology was developed, based upon thin section microscopic counts and an objective varve interpolation programme³⁰. Secondly, the cumulative uncertainty inherent to such layer counting methodologies was reduced through utilising the 639 radiocarbon dates from the varved section of the core and applying a Bayesian Poisson-process deposition model to fit the Suigetsu data onto the independently U–Th dated Hulu Cave radiocarbon calibration dataset³⁶, thus combining the relative dating strength of varves, and the absolute dating precision of U–Th methods³⁴. Finally, the Lake Suigetsu radiocarbon data on

this 'preliminary timescale', along with all of the other contributory datasets, were incorporated into the construction of the IntCal20 consensus radiocarbon calibration curve itself³³. A useful aspect of this methodology is that it directly produces marginal posterior dates (i.e. IntCal20 ages) for the Lake Suigetsu stratigraphy. Accordingly, the IntCal20 chronology for the palaeomagnetic data presented herein is thoroughly robust. The Bayesian age model is transferred to the SG14 core, based on detailed (1 mm-precision) stratigraphic correlations using event layers (e.g. tephra layers) and micro facies captured in high-resolution photographs before oxidation²⁶. The tephra layers can also be used to correlate Suigetsu to other regional records. In particular, there are tephra layers that are stratigraphically located very close to the two excursions and if they are found in other records they could be used as a proxy for the position of the excursions. One, potentially widespread tephra from Changbaishan volcano, on the border of North Korea and China, is identified just below the Laschamp Excursion. This tephra, B-Sg-42, is found at a composite depth of 3378.9–3379.9 cm⁵⁷, which corresponds to a date of 42,580 ± 120 IntCal20 yrs BP, and only 16 cm (~180 years) below the onset of the Laschamp Excursion. Another, the U–Ym tephra (SG14-3216), sits between the Laschamp (90 cm after it ends; ~870 years) and the Post-Laschamp (Suigetsu) Excursion (143 cm below the onset; ~1700 years). It is from an eruption of Ulleungdo Island, South Korea, which is dated to 40,830 ± 120 IntCal20 yrs BP based on its composite depth of 3216.2 m⁵⁷.

The smooth composite depth–age relationship for the discrete samples used for magnetic analyses confirms the highly precise stratigraphic correlations (Fig. 2), except four levels where a small basic resolution (proportional to a reciprocal of s.r.) is estimated between adjacent sample depth/age data, from different-hole core segments or event layers. We could visually count ca. 20 to 25 varves in dry cubic samples around the expected Laschamp horizon after THDs, which is consistent with the mean s.r. of 96 cm/kyr (=ca. 21 yr in 2 cm). For example, we count 22 and 25 annual layers in the dry sample photographs in Fig. 2c, consistent with the basic resolution (Fig. 2b). The durations of excursions episodes estimated by the varve counts of the varve chronology model 2018³⁰ are close to those estimated by the IntCal20 age differences (Table 1). In this study, we use the IntCal20 age model for absolute age estimates and the varve count data for duration estimates for excursions and short episodes.

Filtering of sediment-magnetisation data. Consideration of the filtering (smoothing) effects upon sedimentary magnetic records are essential when comparing the high-resolution Lake Suigetsu palaeomagnetic data with existing lower-resolution datasets. Magnetisation data of sediments measured with a discrete sample suffer two kinds of filters. One is a filter with a box function whose width equals the thickness of a sample. The other is a filter with a lock-in rate function as a result of PDRM processes due to progressive sediment consolidation and dewatering, for which various kinds of functions have been proposed^{23,38–40}. As s.r. decreases, time widths of both functions increase to cause higher filtering effects. We estimate how the high-resolution magnetisation data from Lake Suigetsu sediments, with a mean s.r. of 96 cm/kyr, would be modified in sedimentary archives with a lower s.r. The magnetisation data of Lake Suigetsu are already filtered with a box function with a width of 21-yr (i.e. the mean time span of our 2-cm thick sample), but the estimation of filtering effects upon the data is useful for variations with a wavelength longer than 21-yr. We prepared time-series vector (x , y , z) data using the ChRM directions and the relative palaeointensity values from 42,600 to 41,400 cal BP, a dense-sampling interval. For relative palaeointensity values, we used the value of NRM intensity normalised by magnetic susceptibility of a sample demagnetised at 200 °C ($J_{200\text{ °C}}/\chi_{200\text{ °C}}$). Equally spaced data were generated by condensing densely spaced data and/or linear interpolations for a data blank. The obtained 21-yr resolution time-series data have almost the same structure as the original data except for swing A, in which three densely spaced data were condensed into one. For a filter of a PDRM process, we used an exponential lock-in rate function based on the laboratory-experiment results, $r(z)$; $r(z) = A \exp(-Az)$ ($A = \ln 2/Z_{1/2}$) for $z \geq 0$, and $r(z) = 0$ for $z < 0$ (Supplementary Fig. 6)³⁸. $Z_{1/2}$ is a half lock-in depth where 50% of magnetisation is locked-in (95% of magnetisation is locked-in at $4.3Z_{1/2}$, and 99% at $6.6Z_{1/2}$). $Z_{1/2}$ values smaller than about 2 cm, excluding the thickness of the bioturbation zone, have been estimated for natural fine sediments. A $Z_{1/2}$ value of ≤ 1 cm has been estimated for the fine marine clays of Osaka Bay⁴². Tauxe et al.⁴³ estimated a value of about 2 cm for the so-called lock-in depth, a downward shift of the magnetic polarity reversal boundary, which equals $Z_{1/2}$. Roberts and Winklhofer²³ estimated that 95% of the PDRM is locked in 5 cm below the surface mixed layer, which is equivalent to a value of 1.2 cm for $Z_{1/2}$. These estimates are inconsistent with much larger lock-in depths, e.g. 15 cm⁵⁸ and 21–34 cm⁵⁹. However, the former includes the thickness of the bioturbation (no lock-in) zone, and the latter is probably a lock-in depth of magnetosomal origin magnetites, respectively.

For filtering with a box function with a width of Δt , we condensed the original data to that averaged over Δt every Δt . For filtering with an exponential lock-in rate function, we integrated the original data convolved with the function whose value was set to zero beyond $6.6Z_{1/2}$ (Supplementary Fig. 6).

Data availability

Supplementary data 1 and 2 provide our palaeomagnetic direction and relative palaeointensity data placed upon the IntCal20 chronology. The datasets are also available at PANGEA, <https://issues.pangea.de/browse/PDI-31210>.

Received: 12 July 2021; Accepted: 2 March 2022;

Published online: 04 April 2022

References

- Verosub, K. L. & Banerjee, S. K. Geomagnetic excursions and their paleomagnetic record. *Rev. Geophys. Space Phys.* **15**, 145–155 (1997).
- Guyodo, Y. & Valet, J. P. Global changes in intensity of the Earth's magnetic field during the past 800 kyr (Sint-800). *Nature* **399**, 249–252 (1999).
- Channell, J. E. T., Singer, B. S. & Jicha, B. R. Timing of quaternary geomagnetic reversals and excursions in volcanic and sedimentary archives. *Quat. Sci. Rev.* **228**, 106114 (2020).
- Nowaczyk, N. R., Arz, H. W., Frank, U., Kind, J. & Plessen, B. Dynamics of the Laschamp geomagnetic excursion from Black Sea sediments. *Earth Planet. Sci. Lett.* **227**, 345–359 (2012).
- Bonhommet, N. & Babkine, J. Sur la présence d'aimantations inversées dans la Chaîne des Puys. *C. R. Acad. Sci. Paris* **264**, 92–94 (1967).
- Gillot, P. Y. et al. Age of the Laschamp paleomagnetic excursion revisited. *Earth and Planet. Sci. Lett* **42**, 444–450 (1979).
- Plenier, G., Valet, J.-P., Guérin, G., Lefèvre, J. C. & Carter-Stiglitz, B. Origin and age of the directions recorded during the Laschamp event in the Chaîne des Puys (France). *Earth Planet. Sci. Lett.* **259**, 414–431 (2007).
- Kristjánsson, L. & Gudmundsson, A. Geomagnetic excursions in late-glacial basalt outcrop in south-western Iceland. *Geophys. Res. Lett.* **7**, 337–340 (1980).
- Levi, S. et al. Late Pleistocene geomagnetic excursion in Icelandic lavas: confirmation of the Laschamp excursion. *Earth Planet. Sci. Lett.* **96**, 443–457 (1990).
- Mochizuki, N. et al. Further K–Ar dating and paleomagnetic study of the Auckland geomagnetic excursions. *Earth Planets Space* **59**, 755–761 (2004).
- Ingham, E. et al. Volcanic records of the Laschamp geomagnetic excursion from Mt Ruapehu, New Zealand. *Earth Planet. Sci. Lett.* **472**, 131–141 (2017).
- Lund, S. P., Schwartz, M., Keigwin, L. & Johnson, T. Deep-sea sediment records of the Laschamp geomagnetic field excursion (~ 41,000 calendar years before present). *J. Geophys. Res.* **110**, B04101 (2005).
- Channell, J. E. T. Late Brunhes polarity excursions (Mono Lake, Laschamp, Iceland Basin and Pringle Falls) recorded at ODP Site 919 (Irminger Basin). *Earth Planet. Sci. Lett.* **244**, 378–393 (2006).
- Channell, J. E. T., Hodell, D. A. & Curtis, J. H. ODP Site1063 (Bermuda Rise) revisited: oxygen isotopes, excursions and paleointensity in the Brunhes Chron. *Geochem. Geophys. Geosyst.* **13**, Q02001 (2012).
- Laj, C., Kissel, C. & Roberts, A. P. Geomagnetic field behavior during the Icelandic basin and Laschamp geomagnetic excursions: A simple transitional field geometry? *Geochem. Geophys. Geosyst.* **7**, Q03004 (2006).
- Sun, Y. B., Qiang, X., Liu, Q. S. & Bloemendal, J. Timing and lock-in effect of the Laschamp geomagnetic excursion in Chinese Loess. *Geochem. Geophys. Geosyst.* <https://doi.org/10.1002/2013GC004828> (2013).
- Lascu, I. et al. Age of the Laschamp excursion determined by U–Th dating of a speleothem geomagnetic record from North America. *Geology.* <https://doi.org/10.1130/G37490.1> (2015).
- Lund, S. P., Benson, L., Negrini, R. M., Liddicoat, J. & Mensing, S. A full-vector paleomagnetic secular variation record (PSV) from Pyramid Lake (Nevada) from 47–17 ka: evidence for the successive Mono Lake and Laschamp Excursions. *Earth Planet. Sci. Lett.* **458**, 120–129 (2017).
- Guillou, H. et al. On the age of the Laschamp geomagnetic excursion. *Earth Planet. Sci. Lett.* **227**, 331–343 (2004).
- Valet, J.-P. & Plenier, G. Simulations of a time-varying non-dipole field during geomagnetic reversals and excursions. *Phys. Earth Planet. Int* **169**, 178–193 (2008).
- Leonhardt, R. et al. Geomagnetic field evolution during the Laschamp excursion. *Earth Planet. Sci. Lett.* **278**, 870–895 (2009).
- Thouveny, N. & Creer, K. M. On the brevity of the Laschamp excursion. *Bull. Soc. Geol. Fr.* **6**, 771–780 (1992).
- Roberts, A. P. & Winklhofer, M. Why are geomagnetic excursions not always recorded in sediments? Constraints from post-depositional remanent magnetization lock-in modeling. *Earth Planet. Sci. Lett.* **227**, 345–359 (2004).
- Simon, Q., Thouveny, N., Bourlès, D. L., Valet, J. P. & Bassinot, F. Cosmogenic ¹⁰Be production records reveal dynamics of geomagnetic dipole moment (GDM) over the Laschamp excursion (20–60ka). *Earth Planet. Sci. Lett.* **550**, 116547 (2020).
- Cooper, A. et al. A global environmental crisis 42,000 years ago. *Science* **371**, 811 (2021).
- Nakagawa, T. et al. SG06, a fully continuous and varved sediment core from Lake Suigetsu, Japan: stratigraphy and potential for improving the radiocarbon calibration model and understanding of late Quaternary climate changes. *Quat. Sci. Rev.* **36**, 164–176 (2012).
- Staff, R. A. et al. The multiple chronological techniques applied to the lake Suigetsu (SG06) sediment core. *Boreas* **42**, 1502–3885 (2013).
- Marshall, M. et al. A novel approach to varve counting using μ XRF and X-radiography in combination with thin-section microscopy, applied to the Late Glacial chronology from Lake Suigetsu, Japan. *Quat. Geochron.* **13**, 70–80 (2012).
- Schlolaut, G. et al. An automated method for varve interpolation and its application to the Late Glacial chronology from Lake Suigetsu. *Japan. Quat. Geochron.* **13**, 52–69 (2012).
- Schlolaut, G. et al. An extended and revised Lake Suigetsu varve chronology from ~50 to ~10 ka BP based on detailed sediment micro-facies analyses. *Quat. Sci. Rev.* **200**, 351–366 (2018).
- Bronk Ramsey, C. et al. A complete terrestrial radiocarbon record for 11.2 to 52.8 kyr B.P. *Science* **338**, 370–374 (2012).
- Reimer, P. et al. IntCal13 and Marine13 radiocarbon age calibration curves 0–50,000 Years cal BP. *Radiocarbon* **55**, 1869–1887 (2013).
- Reimer, P. J. et al. The IntCal20 northern hemisphere radiocarbon age calibration curve ((0–55 cal kBP). *Radiocarbon* **62**, 725–757 (2020).
- Bronk Ramsey, C. et al. Reanalysis of the atmospheric radiocarbon calibration record from Lake Suigetsu, Japan. *Radiocarbon* **62**, 989–999 (2020).
- Steinhilber, F. et al. 9,400 years of cosmic radiation and solar activity from ice cores and tree rings. *Proc. Natl Acad. Sci. USA* **109**, 5967–5971 (2012).
- Cheng, H. et al. Atmospheric ¹⁴C/¹²C changes during the last glacial period from Hulu Cave. *Science* **362**, 1293–1297 (2018).
- Cauquoin, A., Raisbeck, G., Jouze, J. & Paillard, D. Use of ¹⁰Be to predict atmospheric ¹⁴C variations during the Laschamp excursion: high sensitivity to cosmogenic isotope production calculations. *Radiocarbon* **56**, 67–82 (2014).
- Hyodo, M. Possibility of reconstruction of the past geomagnetic field from homogeneous sediments. *J. Geomag. Geoelectr.* **36**, 45–62 (1984).
- Roberts, A. P., Tauxe, L. & Heslop, D. Magnetic paleointensity stratigraphy and high-resolution Quaternary geochronology: successes and future challenges. *Quat. Sci. Rev.* **61**, 1–16 (2013).
- Egli, R. & Zhao, X. Natural remanent magnetization acquisition in bioturbated sediment: general theory and implications for relative paleointensity reconstructions. *Geochem. Geophys. Geosyst.* **16**, 995–1016 (2015).
- Bourne, M. D., Niocaill, C. M., Alex, L., Thomas, A. L. & Henderson, G. M. High-resolution record of the Laschamp geomagnetic excursion at the Blake-Bahama Outer Ridge. *Geophys. J. Int.* **195**, 1519–1533 (2013).
- Hyodo, M., Itota, C. & Yaskawa, K. Geomagnetic secular variation reconstructed from wide-diameter cores of Holocene sediments in Japan. *J. Geomag. Geoelectr.* **45**, 669–696 (1993).
- Tauxe, L., Herbert, T., Shackleton, N. J. & Kok, Y. S. Astronomical calibration of the Matuyama–Brunhes boundary: consequences for magnetic remanence acquisition in marine carbonates and the Asian loess sequences. *Earth Planet. Sci. Lett.* **140**, 133–146 (1996).
- Yamazaki, T., Yamamoto, Y., Acton, G., Guidry, E. P. & Richter, C. Rock-magnetic artifacts on long-term relative paleointensity variations in sediments. *Geochem. Geophys. Geosyst.* **14**, 29–43 (2013).
- Gubbins, D. The distinction between geomagnetic excursions and reversals. *Geophys. J. Int.* **137**, F1–F3 (1999).
- Brown, M. C., Korte, M., Holme, R., Wardinski, I. & Gunnarson, S. Earth's magnetic field is probably not reversing. *Proc. Natl Acad. Sci. USA* **115**, 5111–5116 (2018).
- Korte, M., Brown, M. C., Panovska, S. & Wardinski, I. Robust global characteristics of the Laschamp and Mono Lake geomagnetic excursions: results from global field models. *Fron. Earth Sci.* **7**, 86 (2019).
- Liu, J., Nowaczyk, N. R., Panovska, S., Korte, M. & Arz, H. W. The Norwegian–Greenland Sea, the Laschamp and the Mono Lake excursions recorded in a Black Sea sedimentary sequence spanning from 68.9 to 14.5 ka. *J. Geophys. Res.* **125**, e2019JB019225 (2020).
- Yamamoto, Y., Shibuya, H., Tanaka, H. & Hoshizumi, H. Geomagnetic paleointensity deduced for the last 300 kyr from Unzen Volcano, Japan, and the dipolar nature of the Iceland Basin excursion. *Earth Planet. Sci. Lett.* **293**, 236–249 (2010).
- Korte, M. & Constable, C. Improving geomagnetic field reconstructions for 0–3 ka. *Phys. Earth Planet. Int* **188**, 247–259 (2011).
- Gubbins, D. & Bloxham, J. Morphology of the geomagnetic field and implications for the geodynamo. *Nature* **325**, 509–511 (1987).
- Amit, H., Aubert, J. & Hulot, G. Stationary, oscillating or drifting mantle-driven geomagnetic flux patches? *J. Geophys. Res.* **115**, B07108 (2010).
- Singer, B. S. et al. Structural and temporal requirements for geomagnetic field reversal deduced from lava flows. *Nature* **434**, 633–636 (2005).
- Hyodo, M. et al. A centennial-resolution terrestrial climatostratigraphy and Matuyama–Brunhes transition record from a loess sequence in China. *Prog. Earth Planet. Sci.* **7**, 26 (2020).
- Laj, C., Mazaud, A., Weeks, R., Fuller, M. & Herrero-Bervera, E. Geomagnetic reversal paths. *Nature* **351**, 447 (1990).

56. Hoffman, K. Dipolar reversal states of the geomagnetic field and core-mantle dynamics. *Nature* **359**, 789–794 (1992).
57. McLean, D. et al. Refining the eruptive history of Ulleungdo and Changbaishan volcanoes (East Asia) over the last 86 kyr using distal sedimentary records. *J. Volcanol. Geotherm. Res.* **389**, 106669 (2020).
58. Suganuma, Y. et al. ¹⁰Be evidence for delayed acquisition of remanent magnetization in marine sediments: implication for a new age for the Matuyam-Brunhes boundary. *Earth Planet. Sci. Lett.* **296**, 443–450 (2010).
59. Snowball, I. et al. An estimate of 620 post-depositional remanent magnetization lock-in depth in organic rich varved lake sediments. *Global Planet. Change* **110**, 264–277 (2013).
60. Muscheler, R. et al. Changes in the carbon cycle during the last deglaciation as indicated by the comparison of ¹⁰Be and ¹⁴C records. *Earth Planet. Sci. Lett.* **219**, 325–340 (2004).
61. Kristjánsson, L. Paleomagnetic observation on Late Quaternary basalts around Reykjavik and on the Reykjanes peninsula. *SW-Iceland. Jökull* **52**, 21–32 (2003).
62. Shibuya, H., Cassidy, J., Smith, I. E. M. & Itaya, T. A geomagnetic excursion in the Brunhes epoch recorded in New Zealand basalts. *Earth Planet. Sci. Lett.* **111**, 41–48 (1992).
63. Tanaka, H. & Kobayashi, T. Paleomagnetism of the late Quaternary Ontake Volcano, Japan: directions, intensities, and excursions. *Earth Planets Space* **55**, 189–202 (2003).

Acknowledgements

This study was supported by grants 15H02143, 16J10887, 18K03804 and 18H03609 from the Japan Society for the Promotion of Science. Part of this study was performed in collaboration with the Center for Advanced Marine Core Research, Kochi University (reference numbers: 14A023, 15A001, 16A002, 18A014 and 19A020) and with the support of JAMSTEC. The 2014 field campaign to obtain the studied sediment core (Fukui-SG14) was funded by Fukui Prefecture, Japan. We thank Dr. Norbert R. Nowaczyk for supplying numerical data in relation to the Laschamp Excursion. We also acknowledge three reviewers who provided constructive feedback and helped to improve aspects of the paper.

Author contributions

M.H. and T.N. designed the study. M.H., H.M., S.T., B.B. and M.M. performed the magnetic analyses, and M.H. simulated the filtering effects of magnetisations. T.N., R.A.S. and C.B.R. constructed the IntCal20 age model of the SG14 core. K.Y., D.M., V.C.S. and

P.G.A. performed laboratory analyses of the litho- and tephra-stratigraphy. T.N., I.K., K.Y., H.M., J.K., R.A.S., D.M., V.C.S., P.G.A., A.Y. and M.H. contributed to the core sampling and processing. M.H. wrote the manuscript, and all authors reviewed and edited the manuscript.

Competing interests

The authors declare no competing interests.

Additional information

Supplementary information The online version contains supplementary material available at <https://doi.org/10.1038/s43247-022-00401-0>.

Correspondence and requests for materials should be addressed to Masayuki Hyodo.

Peer review information *Communications Earth & Environment* thanks Quentin Simon, Monica Korte and the other, anonymous, reviewer(s) for their contribution to the peer review of this work. Primary Handling Editors: Claire Nichols, Joe Aslin and Heike Langenberg. Peer reviewer reports are available.

Reprints and permission information is available at <http://www.nature.com/reprints>

Publisher's note Springer Nature remains neutral with regard to jurisdictional claims in published maps and institutional affiliations.



Open Access This article is licensed under a Creative Commons Attribution 4.0 International License, which permits use, sharing, adaptation, distribution and reproduction in any medium or format, as long as you give appropriate credit to the original author(s) and the source, provide a link to the Creative Commons license, and indicate if changes were made. The images or other third party material in this article are included in the article's Creative Commons license, unless indicated otherwise in a credit line to the material. If material is not included in the article's Creative Commons license and your intended use is not permitted by statutory regulation or exceeds the permitted use, you will need to obtain permission directly from the copyright holder. To view a copy of this license, visit <http://creativecommons.org/licenses/by/4.0/>.

© The Author(s) 2022

Suigetsu 2014 Project

Gordon Schlolaut¹⁰, Katsuya Gotanda¹¹, Kosuke Tsumura², Kaito Inagawa², Koyo Kumazawa², Haruka Abe², Saki Sugo¹¹, Koki Takahashi¹¹ & Atsumi Kitamura¹²

¹⁰GFZ German Research Centre for Geosciences, Telegrafenberg, 14473 Potsdam, Germany. ¹¹Chiba University of Commerce, Ichikawa, Chiba 272-8512, Japan. ¹²Seibushisui Co. Ltd., Tokitsu, Nagasaki 851-2108, Japan.